Theory of cell size regulation underlying the onset of migration in adhered cells

Jonathan E. Ron [1,2,*] and Ram M. Adar [1,†]

[1]*Department of Physics, Technion—Israel Institute of Technology, Haifa 32000, Israel*

[2]*Department of Chemical and Biological Physics, Weizmann Institute of Science, 234 Herzl Street, Rehovot 7610001, Israel*

(Received 29 May 2025; accepted 11 December 2025; published 20 January 2026)

Cell migration is closely linked to cell shape, yet cell size is often assumed to remain constant. This assumption is challenged by recent experiments showing that cells undergo volume loss during spreading and swelling upon activation, with migration velocity correlated to cell size. In this work, we present a minimal theoretical framework for cellular size regulation and its influence on migration velocity. We connect cell size to membrane potential and active, actin-driven forces. Spatial inhomogeneities in these forces establish cell polarization and drive migration. Crucially, inhomogeneity is easier to establish over larger sizes, giving rise to a critical contact area, above which migration is possible. Our theory captures the coupled dynamics of cell volume, surface area, and motility and explains recent experiments on neutrophils.

DOI: 10.1103/1gkb-qs3z

I. INTRODUCTION

Cellular migration underlies fundamental biological processes such as development, immune response, and metastasis [1–3]. From a biophysical perspective, migration requires both a driving force—typically associated with actin polymerization—and a well-defined polarization that determines the direction of motion [4].

The role of cellular shape changes during migration is well established: Asymmetry facilitates polarization and supports persistence [5–12]. In contrast, the cell size is often assumed to remain constant [13]. However, this assumption breaks down even on short timescales, as cells undergo significant water exchange within seconds and ion transport within minutes [14]. Recent studies have shown that cells lose volume during spreading [15–17], a phenomenon attributed to mechanosensitive ion channels that open in response to increased surface tension [15,17–19]. Adhered neutrophils have also been observed to swell [20–22] upon chemoattractant exposure via ion channel activation, with migration velocity increasing during swelling [22].

In this work, we elucidate the coupled dynamics of cell volume and contact area, and their impact on migration over an adhesive substrate. First, we describe volume regulation using the pump-leak model for water and ion transport. Second, we relate spreading dynamics to the interplay between actin-driven protrusive forces and membrane surface tension. Together, volume and spreading determine the contact area of the cell. Finally, we demonstrate that contact area directly influences migration: Polarization arises from gradients in actin-regulatory components, which are more readily established across larger domains. This leads to a critical contact area above which persistent migration is possible.

Our theory offers a coherent framework for the interdependent roles of electrochemical regulation, cellular mechanics, and motility, and quantitatively captures recent experimental findings on neutrophil migration following activation.

II. THEORY OF CELL VOLUME AND AREA

We consider a simplified model of an adhered cell that adopts the shape of a spherical cap (Fig. 1). The cell interior is modeled as a solution, comprising of water, ions that exchange with the extracellular environment, and impermeant molecules, including proteins that interact with cortical actin and act as polarity cues (Fig. 1).

Next, we apply this model to derive coupled equations for cellular volume, contact angle, and migration velocity.

A. Cell volume

We find the cellular volume V via the pump-leak model [23–25], which accounts for active ion transport through pumps and passive leakage through ion channels (see the Supplemental Material [26]). The volume is determined by osmotic pressure balance with the extracellular environment and is given by [18,19,27]

$$V(t) = V_d + \frac{V_m - V_d}{1 - e^{\psi(t)}}. \tag{1}$$

Here, V_d is the dry cellular volume due to the impermeant molecules and intracellular membrane (obtained at infinite extracellular pressure) and V_m is the minimal possible volume in isotonic conditions, obtained when the cell contains only the

*Contact author: jonathan.ron@weizmann.ac.il

†Contact author: radar@technion.ac.il

Published by the American Physical Society under the terms of the Creative Commons Attribution 4.0 International license. Further distribution of this work must maintain attribution to the author(s) and the published article's title, journal citation, and DOI.

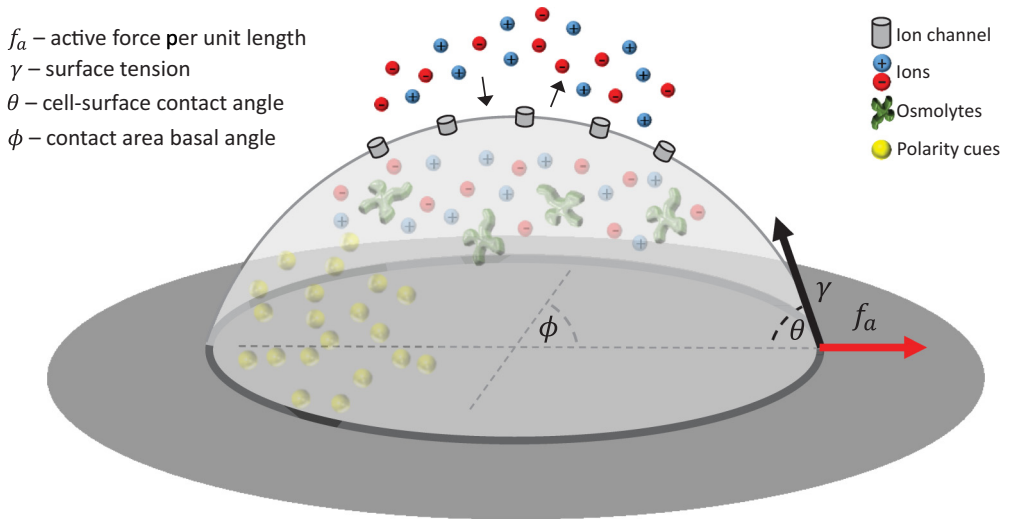

FIG. 1. Model illustration. An adhered cell is represented by a spherical cap. An active force per unit length f_a acts outwardly along the contact ring and is opposed by the cellular surface tension γ. The angle θ is the cell-substrate contact angle. The angle ϕ is the azimuthal angle along the contact ring. Red and blue mark ions that exchange with the extracellular environment. Green marks impermeant molecules. Yellow marks actin polarity cues.

impermeant molecules and their counterions. The contribution of additional ions is tuned by the dimensionless membrane potential $\psi < 0$. Note that for extremely hyperpolarzied cells ($\psi \ll -1$), the additional ions escape the cell and $V = V_m$, while extreme depolarization ($\psi \approx 0$) leads to very large volumes and, practically, cell rupture.

The membrane potential maintains intracellular electroneutrality. Its value is determined by the ionic pump rates and passive conductances, as well as the intracellular and extracellular ionic concentrations. We consider two sources of potential dynamics: (1) mechano-sensitive (stretch-activated) channels that open during spreading due to increased surface tension [15,17–19,28] and (2) channel activation as part of regulatory volume increase (RVI). The latter is relevant to volume adaptation after hypertonic osmotic shocks [20,29] and upon exposure of neutrophils to chemoattractants [22]. For simplicity, we consider instantaneous adaption of the channels.

Within linear response, the potential evolves as (see the Supplemental Material [26])

$$\psi(t > 0) = \psi_0 - \delta_1 \frac{\gamma(t) - \gamma_0}{\gamma_0} - \delta_2 \mathrm{e}^{-t/\tau_\psi}. \tag{2}$$

where ψ_0 is the steady-state value after long times, δ_1 accounts for mechanosensitivity, $\gamma(t)$ is the cellular surface tension, and γ_0 is the steady-state tension at rest. δ_2 is the change in potential due to activation, while τ_ψ is the typical membrane potential adaptation time, related to the leakage of cellular cations [27]. Linear response is justified by the relatively small potential changes that correspond to experimentally measured volume changes [27]. Throughout this paper, we focus on the case of $\delta_1 > 0$, which is supported by experimental evidence from four independent studies [15–17,22] on various cells, indicating that membrane potential (and hence, cellular volume) decreases with increasing tension. We also focus on $\delta_2 > 0$, relevant for regulatory volume increase. Under these conditions, the cell swells over a period of τ_ψ.

B. Cell contact area

We consider an adhered cell with the shape of a spherical cap (Fig. 1). Its contact area is set by its volume and contact angle θ. The latter is determined by a balance of forces acting on the cell periphery, as in Young's law. The apical (cell-medium) surface tension γ exerts a force per unit length tangentially to the cell surface. Its projection on the basal plane, $\gamma \cos\theta \equiv \gamma\,\Theta$, is balanced by the difference of medium-substrate and cell-substrate tensions, $\gamma_{\mathrm{ms}} - \gamma_{\mathrm{cs}}$. We denote the difference $\gamma + \gamma_{\mathrm{ms}} - \gamma_{\mathrm{cs}} = f_a$, which quantifies how much a cell tends to spread on a substrate.

For a homogeneous substrate, as considered throughout this paper, f_a does not depend on the cellular position. It is determined mostly by cell-substrate interaction via polymerization and adhesion bonds. We focus on polymerization, and consider f_a hereafter as an effective active force that acts in the normal direction away from the cell.

At long times, therefore, we obtain a contact angle of

$$\Theta = \frac{f_a}{\gamma} - 1. \tag{3}$$

At shorter times that are of interest to us, we assume linear-response dynamics, whereby Θ relaxes toward steady state with a finite relaxation time τ_θ,

$$\left(1 + \tau_\theta \frac{\mathrm{d}}{\mathrm{d}t}\right)\Theta(t) = \frac{f_a}{\gamma(t)} - 1. \tag{4}$$

Cellular tension also varies with time. For simplicity, we assume tension homeostasis at long times, with a transient viscoelastic contribution (Maxwell model)

$$\left(1 + \tau_\gamma \frac{\mathrm{d}}{\mathrm{d}t}\right)\gamma(t) = \gamma_0 + \eta \frac{\mathrm{d}}{\mathrm{d}t}\epsilon(t). \tag{5}$$

Here, τ_γ is the viscoelastic relaxation time, η is the viscosity, and $\epsilon(t)$ is the strain $(A_{\mathrm{tot}}(t) - A_0)/A_0$, defined with respect to the total cell area A_{tot} (sum of contact and apical areas)

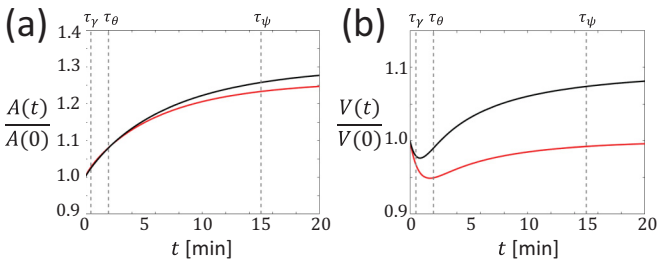

FIG. 2. Spreading and swelling dynamics, with/without RVI (black/red curve). (a) Normalized contact area. (b) Normalized volume. Vertical dashed lines indicate the elastic, spreading, and potential activation timescales (τ_γ, τ_θ, and τ_ψ, respectively). Parameters: $\tau_\gamma, \tau_\theta, \tau_\psi = 0.5, 2, 15$ (min); $\psi_0, \delta_1 = -1.03, 4$ and $\delta_2 = 1.4$ (black) or 0 (red); $f_a/\gamma_0 = 1.83$; $\eta A(0)/\tau_\gamma\gamma_0 = 4.8$; $V_d = 0.3V(0)$, $V_m = 2.5V_d$; $A(0) = 154$ (μm^2); and $V(0) = 250$ (μm^3).

and reference area A_0. This model for the membrane tension is supported by direct measurements conducted on fibroblasts [30] and measurements of transient volume loss during spreading [17], attributed to tension changes.

The contact area is related to the contact angle and volume by the spherical cap approximation

$$A = (9\pi)^{1/3}\frac{V^{2/3}(1+\Theta)}{(2+\Theta)^{2/3}(1-\Theta)^{1/3}}. \tag{6}$$

The contact area dynamics are similarly related to the volume and contact angle via the chain rule,

$$\frac{dA}{dt} = \frac{\partial A}{\partial V}\bigg|_\Theta \frac{dV}{dt} + \frac{\partial A}{\partial \Theta}\bigg|_V \frac{d\Theta}{dt}. \tag{7}$$

The first term represents area changes driven by volume changes (swelling), while the second term corresponds to area changes due to contact angle variations (spreading).

C. Volume-area coupling

The interplay between volume and area [Eqs. (1)–(7)] is governed by two processes: (1) tension-driven volume loss (δ_1 term) and (2) regulatory volume increase (δ_2 term) driven by ion transport activity. Concurrently, the tension depends on the cellular area, which itself depends on volume [Eq. (6)]. Our description applies for timescales longer than the typical timescale of water permeation (∼1 s) and of Cl^- leakage [27], which are assumed to be shorter than the typical spreading time (∼1 min). In addition, we limit ourselves to timescales shorter than an hour, when further regulatory mechanisms become important, such as protein synthesis.

Note that the interplay between volume and area can lead to an instability. It arises only when δ_1 is sufficiently negative (see the Supplemental Material [26]), i.e., when cells *gain* volume upon spreading. In this scenario, small fluctuations in cellular volume increase the area, which, in turn, amplifies the volume due to its tension dependence.

We numerically solve Eqs. (1)–(7) to predict the volume and area dynamics upon activation, as is illustrated in Fig. 2. We model activation as a sudden increase in the active force f_a at $t = 0$ and consider both $\delta_2 = 0$ (no RVI) and $\delta_2 > 0$ (RVI). The dynamics are governed by the three timescales introduced above. The increase in active force leads to an increase in Θ (spreading) and, consequently, increase in area. The timescale of this process is $\sim\tau_\theta$. During spreading, the tension transiently increases, reaching a maximum within a time comparable to τ_γ. Simultaneously, the volume decreases due to mechanosensitivity (δ_1 term). Given RVI, the membrane potential increases during a time comparable with τ_ψ leading to an increase in volume (swelling). Swelling also increases the contact area, while Θ remains unaffected.

This establishes the volume and area dynamics due to the combination of spreading and swelling. Next, we show how the migration velocity is largely determined by the contact area.

III. CRITICAL CONTACT AREA AND MIGRATION VELOCITY

The migration velocity u is determined by the balance between friction and active forces on the cellular scale,

$$2\pi\Gamma(R)u = \int_0^{2\pi} f_a(\phi)\cos\phi\, d\phi. \tag{8}$$

We define the friction coefficient per unit length $\Gamma(R)$ and allow further dependence on the basal area via

$$\Gamma(R) = \Gamma_0\left(\frac{R}{R_0}\right)^\alpha, \tag{9}$$

where Γ_0 is a reference value, $R = \sqrt{A/\pi}$ is the radius of the basal area, and R_0 is a reference value of the radius (of order 1 μm). The power α accounts for the leading-order dependence on the radius. It varies between perimeter-dominated ($\alpha = 0$) friction and area-dominated friction ($\alpha = 1$).

As long as the active force distribution $f_a(\phi)$ is homogeneous, there is no net force and $u = 0$. Cell migration requires an inhomogeneous force distribution, i.e., polarization. In the absence of external fields, polarization can be obtained by a spontaneous symmetry breaking of an internal cellular degree of freedom. In our model, this degree of freedom corresponds to the concentration of "polarity cues"—proteins that regulate actin protrusions along the cell contact ring in the outward normal direction. We consider generic polarity cues that can represent, for example, membrane curvature regulators such as IRSp53 [31,32], actin-polymerization inhibitors such as arpin [5,33,34], capping proteins [35], or signaling molecules that promote protrusive activity such as Rac1 [36–38].

Cellular polarization emerges in our theory from a generic feedback between cellular migration and advection of polarity cues. Similar theories have been successful in capturing key features of cell migration across different cell types [5,11,34,39,40]. The polarity cues diffuse within the cytoplasm with a diffusion coefficient D and are advected by the net retrograde cytoplasmic flow, which is assumed to be proportional and opposite to the migration velocity [34,41,42]. The interplay between diffusion and advection skews the polarity cue distribution along the direction of motion (chosen hereafter as the x direction), driving migration self-consistently. This interplay is characterized by the Péclet number $\tilde{u} = uR/D$. Based on these arguments, we write the distribution of active forces as

$$f_a(\phi) = f_0[1 + p(\tilde{u}\cos\phi)], \tag{10}$$

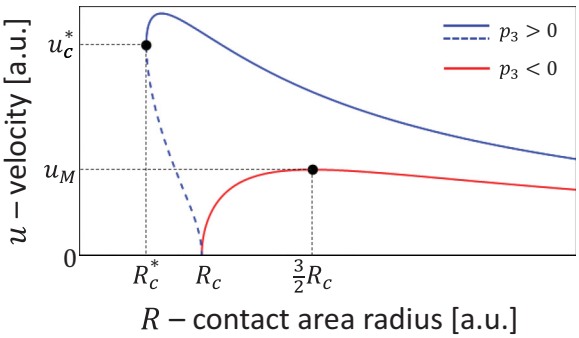

FIG. 3. Migration velocity as a function of contact radius [Eq. (13)]. The red (blue) curve indicates the solution for $p_3 > 0$ ($p_3 < 0$). Solid (dashed) lines indicate the stable (unstable) branches. Parameters: $\Gamma D/f_0 = 1.12$ (μm) and $p_3 = \pm 1$.

where f_0 is an intrinsic scale of force per unit length and p accounts for the anisotropy in the distribution of polarity cues. We assume that $p \ll 1$, such that its effect on spreading is negligible [Eq. (4)].

Next, we insert this expression in the force balance equation [Eq. (8)] and solve for $\tilde{u}$. Due to the many arguments that enter p (such as the protein-membrane interaction, intracellular transport, and force generation), we phenomenologically expand it in powers of $\tilde{u}$:

$$\frac{\Gamma(R)D}{f_0 R}\tilde{u} = \frac{1}{2\pi}\int_0^{2\pi} p(\tilde{u}\cos\phi)\cos\phi\, d\phi \approx p_1\tilde{u} + p_3\tilde{u}^3 + p_5\tilde{u}^5, \tag{11}$$

where p_n are the polynomial coefficients. The cell size enters Eq. (11) through the radius R and consequently affects the migration velocity. Its effect is twofold: (1) It enters the prefactor on the left-hand side and acts similar to an inverse temperature near a phase transition and (2) it defines the typical migration speed magnitude according to $u = \tilde{u}D/R$.

We analyze the possible values of $\tilde{u}$ as a function of R and the coefficients p_n. We assume that $p_1 > 0$ and $p_5 < 0$, allowing for the truncation of the expansion. The velocity behavior largely depends on the sign of p_3 (illustrated in Fig. 3).

For $p_3 < 0$, we neglect p_5 and Eq. (11) reduces to a quadratic equation for $\tilde{u}$. We solve it (see the Supplemental Material [26]) and find that $\tilde{u} = 0$ for small radii and smoothly increases $\tilde{u} \geqslant 0$ beyond the critical radius of

$$R_c = \left(\frac{\Gamma_0 D}{f_0 p_1 R_0^{\alpha}}\right)^{\frac{1}{1-\alpha}}. \tag{12}$$

Equation (12) demonstrates that the critical size for migration is smaller for stronger driving, active forces (f_0) and lower relaxation of polarization and migration (related to D and Γ_0, respectively). The friction exponent α is also important. The critical radius R_c is finite for $0 \leqslant \alpha < 1$ and diverges in the limit $\alpha \to 1$. This is evident from the left-hand side of Eq.(11), which becomes size independent in this limit.

Traction force measurements demonstrate a nonuniform distribution of forces that tend to concentrate near the leading edge during migration [43–45], as well as localization of adhesion complexes at the cell periphery during cell spreading [46]. These findings are consistent with $\alpha \gtrsim 0$ that—according to Eq. (12)—allow for a transition between stationary and migrating cells. For simplicity, we refer to the case of $\alpha = 0$ hereafter. Calculations for a general $0 < \alpha < 1$ yield the same qualitative behavior close to the transition (see the Supplemental Material [26]).

For $p_3 > 0$, Eq. (11) reduces to a quadratic equation for $\tilde{u}^2$. Its solution is $\tilde{u} = 0$ for $R < R_c^*$, with $R_c^* = R_c/(1 + p_3^2/4p_1|p_5|) < R_c$, above which there is a sudden jump to $\tilde{u} = u_c^* R/D > 0$. This discontinuous transition corresponds to a subcritical bifurcation (Fig. 3 and see the Supplemental Material [26]). In both cases, $\tilde{u}$ increases with R. However, as $u = \tilde{u}D/R$, the actual velocity exhibits a maximum and decreases with R for large radii (Fig. 3). Explicitly, the velocity is given by

$$u = \begin{cases} \frac{3^{3/2}}{2} u_M \frac{R_c}{R}\sqrt{1 - \frac{R_c}{R}}, & p_3 < 0,\ R > R_c, \\ u_c^* \frac{R_c^*}{R}\sqrt{1 \pm \sqrt{\frac{R_c}{R_c - R_c^*}\left(1 - \frac{R_c^*}{R}\right)}}, & p_3 > 0,\ R > R_c^*, \end{cases} \tag{13}$$

and vanishes for lower values of R. In the case $p_3 < 0$, u_M is the maximal velocity, obtained for $R = 3R_c/2$. For $p_3 > 0$, the transition occurs at $u = u_c^*$ for $R = R_c^*$. There are two branches (Fig. 3): a stable branch that increases with R until a maximum (plus sign in the square root) and an unstable branch that decreases with R and vanishes for $R = R_c$ (minus sign in the square root). For the full derivation of Eq. (13), see the Supplemental Material [26].

Our results explain the size dependence of the migration speed in a simple manner: migration requires polarization, achieved within our theory via a gradient of polarity cues along the contact ring. Gradients are easier to establish over larger distances inside the cell, leading to an increase in velocity as the contact area increases. A similar result was obtained in a 1D model of cellular migration [5,34]. As polarization is linked within our theory to $\tilde{u} = uR/D$, the velocity decreases with area once maximal polarization is established. This occurs at relatively large radii ($R = 3R_c/2$ in the continuous case), which are not necessarily achievable experimentally. We restrict our discussion hereafter to cell sizes close to the transition, where the velocity increases with radius. In these settings, the shape asymmetry of polarized cells, which is not the focus of this work, is negligible.

Finally, we highlight that even stationary cells ($u = 0$) are expected to diffuse randomly. Our theory captures this effect by considering anisotropic fluctuations in the polarity cue distribution, which modify Eq. (10), according to $f_a(\phi) = f_0[1 + p(\tilde{u}\cos\phi) + p_\xi(\phi)]$, where $p_\xi(\phi)$ represents a Gaussian white noise. This provides a correction to the velocity u_ξ with $\langle u_\xi \rangle = 0$ and $\langle u_\xi^2 \rangle \sim (f_0/\Gamma)^2$. Interestingly, this result relates the critical area $A_c = \pi R_c^2$ with the mean-squared velocity during diffusion $A_c \sim 1/\langle u_\xi^2 \rangle$. The relation between the critical area and velocity fluctuations in the nonmotile case can be tested experimentally.

IV. COMPARISON WITH EXPERIMENTS

We compare our theoretical predictions with recent experiments by Nagy *et al.* [22] where neutrophils were

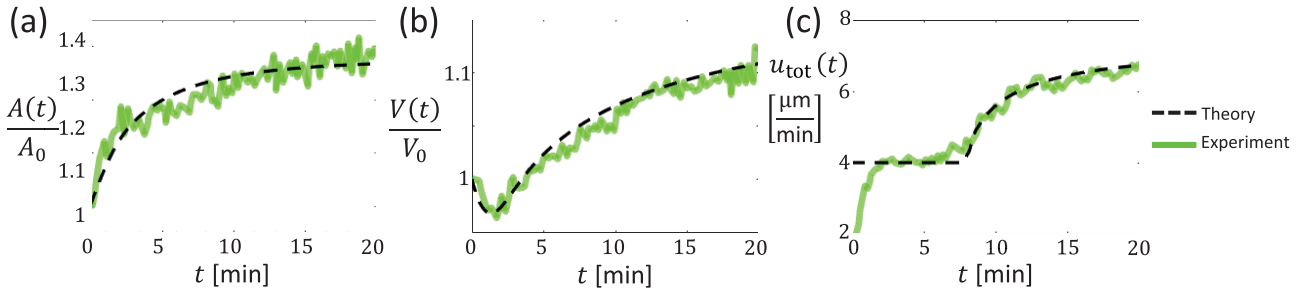

FIG. 4. Comparison between theory (dashed black) and neutrophil experiments [22] (green), upon chemoattractant exposure at $t = 0$. (a) Normalized area. (b) Normalized volume. (c) Cell velocity. Parameters: $\tau_\gamma, \tau_\theta, \tau_\psi = 0.85, 0.85, 12$ (min);. $\psi_0, \delta_1, \delta_2 = -1.53, 0.75, 0.08$; $f_0/\gamma_0 = 1.47, 1.96$ (pre/post activation); $\eta/\gamma_0 = 0.54\tau_\gamma/A_0$; $\Gamma D/f_0 = 0.34, 0.26$ (μm) (pre/post activation); $p_1, p_3 = 0.033, 10^{-6}$; and $V_d = 0.3V_0$, $V_m = 2.5V_d$. Initial conditions: $A_0 = 154$ (μm^2), $V_0 = 250$ (μm^3), and $\Theta_0 = 0.44$.

simultaneously and uniformly exposed to chemoattractants. For each cell, velocity was inferred from tracking, contact area was measured directly, and volume was quantified using fluorescence exclusion microscopy [22,47]. We summarize key experimental findings and interpret them through our theory. As shown in Fig. 4, our predictions show excellent agreement with the measurements.

A. Cell spreading and swelling

Upon chemoattractant exposure, cells undergo spreading followed by swelling (Fig. 4). Spreading occurs within minutes, where the contact area increases by ∼10%, and the volume decreases by ∼5%. Swelling occurs during the following 15 min, where the contact area increases by an additional 20%, while the volume increases by approximately 15% above the initial level. The swelling was suppressed upon inhibition of NHE1 exchangers [22], which play an important role in RVI [20,21,29].

Our theory intuitively explains these findings. We model the response to chemoattractants via two primary drivers of cell dynamics in our theory: (1) a sudden increase in active force f_0 and (2) a rapid change in ion conductances, resulting in an adaptation of the membrane potential δ_2 term in Eq. (2). The combination of these effects drives an increase in cellular area, as described by Eq. (7) and depicted in Fig. 2(b). Most of the spreading occurs on a timescale of $\sim\tau_\theta$, during which the volume decreases due to mechanosensitivity [δ_1 term in Eq. (2)]. Over longer timescales, on the order of τ_ψ, the volume increases due to membrane potential regulation ($\delta_2 > 0$).

B. Cell migration

The experiments also reveal notable behavior in cell velocity. Prior to chemoattractant exposure, cells move randomly with a typical velocity of about 2 μm/min [22]. This motion corresponds to a random velocity u_ξ that is possible even for $u = 0$ due to active force fluctuations (discussed above). Upon exposure, the velocity increases and reaches a plateau twice as large as the initial random speed [Fig. 4(c)], for about 10 min. During this time, the cellular motion remains relatively random with low persistence. We regard this as a change in u_ξ, whose modeling lies beyond the scope of this work.

About 10 min into this plateau, the cellular velocity increases with time, as the cell continues to swell. Cellular persistence also increases. We interpret this behavior as the onset of persistent migration with $u > 0$, where the total velocity observed in the experiments is $u_{\mathrm{tot}} = \sqrt{u^2 + u_\xi^2}$. The increase in velocity is explained by the increase in contact area during swelling [Fig. 4(a)], according to Eq. (13). Explicitly, we consider a critical contact area of $A_c \approx 1.3\,A$ ($t = 0$). Once this value is achieved, u smoothly increases with the contact area, explaining the observed behavior. The velocity is monotonically increasing, since the maximal velocity is predicted for $A = 9A_c/4$, which was not reached in the experiments. Importantly, these findings highlight that swelling promotes faster migration by increasing the contact area rather than the volume.

V. DISCUSSION

This work introduces a minimal framework to elucidate cellular size regulation during migration, predicting distinct regimes of migration velocity and its dependence on cell size, including a critical contact area for migration. Our predictions can be tested experimentally by simultaneously tracking cell position, contact area, and volume across various cell types.

Our theory provides an explanation for the increase in migration speed of neutrophils upon swelling, as reported by Nagy *et al.* [22]. Swollen cells exhibit larger contact areas, facilitating higher polarization, which in turn increases migration speed and persistence. Crucially, it is the increase in contact area that promotes the increase in cell speed, rather than the water content linked to cell volume, as previously suggested. To validate this interpretation, we examined the correlation between neutrophil migration velocity, volume, and contact area (see the Supplemental Material [26]). Our findings indicate that migration velocity correlates more strongly with contact area than with volume, supporting our theoretical predictions.

To further evaluate the prediction of a critical cell area, we propose two complementary experimental approaches to manipulate the ratio A/A_c. In the first, the cell area would be systematically varied while cell volume and the presumed determinants of a critical area remain approximately fixed. This is possible, for instance, using geometric

confinement. In the second, the factors that set the critical area would be selectively perturbed. This can be done by manipulating intracellular transport or cell–substrate adhesion, combined with additional constraints to hold cell dimensions constant.

Our theory distinguishes between two primary drivers of cell size: membrane potential and active forces. The membrane potential varies with volume and area simultaneously, following the scaling $A \sim V^{2/3}$. In contrast, active forces modulate the contact angle and produce an opposing trend between volume and area. An increase in f_0 increases the contact area while reducing cellular volume, mediated by ion channels' mechanosensitivity. This key distinction should be useful in the interpretation of cellular volume and area dynamics on the scale of minutes.

This study advances our understanding of the interplay between electrophysiology and mechanics in regulating the concurrent dynamics of cell size and migration. Further experiments across different cell types are required to fully uncover this coupling.

ACKNOWLEDGMENT

We thank Nir S. Gov, Kinneret Keren, Tamas L. Nagy, Samuel A. Safran, and Orion D. Weiner for useful discussions.

DATA AVAILABILITY

The data that support the findings of this article are openly available [22].

[1] P. Friedl and D. Gilmour, Collective cell migration in morphogenesis, regeneration and cancer, Nat. Rev. Mol. Cell Biol. **10**, 445 (2009).

[2] P. Friedl and S. Alexander, Cancer invasion and the microenvironment: Plasticity and reciprocity, Cell **147**, 992 (2011).

[3] S. Nourshargh and R. Alon, Leukocyte migration into inflamed tissues, Immunity **41**, 694 (2014).

[4] V. Hakim and P. Silberzan, Collective cell migration: A physics perspective, Rep. Prog. Phys. **80**, 076601 (2017).

[5] J. E. Ron, P. Monzo, N. C. Gauthier, R. Voituriez, and N. S. Gov, One-dimensional cell motility patterns, Phys. Rev. Res. **2**, 033237 (2020).

[6] J. E. Ron, M. Crestani, J. M. Kux, J. Liu, N. Al-Dam, P. Monzo, N. C. Gauthier, P. J. Sáez, and N. S. Gov, Emergent seesaw oscillations during cellular directional decision-making, Nat. Phys. **20**, 501 (2024).

[7] J. Liu, J. Boix-Campos, J. E. Ron, J. M. Kux, N. S. Gov, and P. J. Sáez, Shape dynamics and migration of branched cells on complex networks, arXiv:2404.00118

[8] M. K. Driscoll, C. McCann, R. Kopace, T. Homan, J. T. Fourkas, C. Parent, and W. Losert, Cell shape dynamics: From waves to migration, PLoS Comput. Biol. **8**, e1002392 (2012).

[9] C. Blanch-Mercader and J. Casademunt, Spontaneous motility of actin lamellar fragments, Phys. Rev. Lett. **110**, 078102 (2013).

[10] D. L. Bodor, W. Pönisch, R. G. Endres, and E. K. Paluch, Of cell shapes and motion: The physical basis of animal cell migration, Dev. Cell **52**, 550 (2020).

[11] I. Lavi, N. Meunier, R. Voituriez, and J. Casademunt, Motility and morphodynamics of confined cells, Phys. Rev. E **101**, 022404 (2020).

[12] R. K. Sadhu, A. Iglič, and N. S. Gov, A minimal cell model for lamellipodia-based cellular dynamics and migration, J. Cell Sci. **136**, jcs260744 (2023).

[13] A. C. Callan-Jones and R. Voituriez, Active gel model of amoeboid cell motility, New J. Phys. **15**, 025022 (2013).

[14] C. Cadart, L. Venkova, P. Recho, M. C. Lagomarsino, and M. Piel, The physics of cell-size regulation across timescales, Nat. Phys. **15**, 993 (2019).

[15] K. Xie, Y. Yang, and H. Jiang, Controlling cellular volume via mechanical and physical properties of substrate, Biophys. J. **114**, 675 (2018).

[16] M. Guo, A. F. Pegoraro, A. Mao, E. H. Zhou, P. R. Arany, Y. Han, D. T. Burnette, M. H. Jensen, K. E. Kasza, J. R. Moore, F. C. Mackintosh, J. J. Fredberg, D. J. Mooney, J. Lippincott-Schwartz, and D. A. Weitz, Cell volume change through water efflux impacts cell stiffness and stem cell fate, Proc. Nat. Acad. Sci. USA **114**, E8618 (2017).

[17] L. Venkova, A. S. Vishen, S. Lembo, N. Srivastava, B. Duchamp, A. Ruppel, A. Williart, S. Vassilopoulos, A. Deslys, J.-M. G. Arcos, *et al.*, A mechano-osmotic feedback couples cell volume to the rate of cell deformation, eLife **11**, e72381 (2022).

[18] R. M. Adar and S. A. Safran, Active volume regulation in adhered cells, Proc. Natl. Acad. Sci. USA **117**, 5604 (2020).

[19] R. M. Adar, A. S. Vishen, J.-F. Joanny, P. Sens, and S. A. Safran, Volume regulation in adhered cells: Roles of surface tension and cell swelling, Biophys. J. **122**, 506 (2023).

[20] E. Delpire and K. B. Gagnon, Water homeostasis and cell volume maintenance and regulation, Curr. Top. Membr. **81**, 3 (2018).

[21] Q. Ni, Z. Ge, Y. Li, G. Shatkin, J. Fu, A. Sen, K. Bera, Y. Yang, Y. Wang, Y. Wu, *et al.*, Cytoskeletal activation of NHE1 regulates mechanosensitive cell volume adaptation and proliferation, Cell Rep. **43**, 114992 (2024).

[22] T. L. Nagy, E. Strickland, and O. D. Weiner, Neutrophils actively swell to potentiate rapid migration, Elife **12**, RP90551 (2024).

[23] D. Tosteson and J. Hoffman, Regulation of cell volume by active cation transport in high and low potassium sheep red cells, J. Gen. Physiol. **44**, 169 (1960).

[24] J. Keener and J. Sneyd, *Mathematical Physiology: I: Cellular Physiology* (Springer Science & Business Media, New York, 2010).

[25] A. R. Kay, How cells can control their size by pumping ions, Front. Cell Dev. Biol. **5**, 41 (2017).

[26] See Supplemental Material at http://link.aps.org/supplemental/10.1103/1gkb-qs3z for the derivation of Eqs. (1), (2), and (13), and the details of the calculations presented in this article.
[27] R. M. Adar, Separation of ionic timescales explains dynamics of cellular volume regulation, Biophys. J. **124**, 1944 (2025).
[28] R. Phillips, J. Kondev, and J. Theriot, *Physical Biology of the Cell* (Garland Science, New York, 2009).
[29] E. K. Hoffmann, I. H. Lambert, and S. F. Pedersen, Physiology of cell volume regulation in vertebrates, Physiol. Rev. **89**, 193 (2009).
[30] N. C. Gauthier, M. A. Fardin, P. Roca-Cusachs, and M. P. Sheetz, Temporary increase in plasma membrane tension coordinates the activation of exocytosis and contraction during cell spreading, Proc. Natl. Acad. Sci. USA **108**, 14467 (2011).
[31] G. Scita, S. Confalonieri, P. Lappalainen, and S. Suetsugu, IRSp53: Crossing the road of membrane and actin dynamics in the formation of membrane protrusions, Trends Cell Biol. **18**, 52 (2008).
[32] A. Mukherjee, J. E. Ron, H. T. Hu, T. Nishimura, K. Hanawa-Suetsugu, B. Behkam, Y. Mimori-Kiyosue, N. S. Gov, S. Suetsugu, and A. S. Nain, Actin filaments couple the protrusive tips to the nucleus through the I-BAR domain protein IRSp53 for migration of elongated cells on 1D fibers, Adv. Sci. (Weinh) **10**, 2207368 (2025).
[33] I. Dang, R. Gorelik, C. Sousa-Blin, E. Derivery, C. Guérin, J. Linkner, M. Nemethova, J. G. Dumortier, F. A. Giger, T. A. Chipysheva, *et al.*, Inhibitory signalling to the Arp2/3 complex steers cell migration, Nature (London) **503**, 281 (2013).
[34] P. Maiuri, J.-F. Rupprecht, S. Wieser, V. Ruprecht, O. Bénichou, N. Carpi, M. Coppey, S. De Beco, N. Gov, C.-P. Heisenberg, *et al.*, Actin flows mediate a universal coupling between cell speed and cell persistence, Cell **161**, 374 (2015).
[35] C. Yang, M. Pring, M. A. Wear, M. Huang, J. A. Cooper, T. M. Svitkina, and S. H. Zigmond, Mammalian CARMIL inhibits actin filament capping by capping protein, Dev. Cell **9**, 209 (2005).
[36] M. Machacek, L. Hodgson, C. Welch, H. Elliott, O. Pertz, P. Nalbant, A. Abell, G. L. Johnson, K. M. Hahn, and G. Danuser, Coordination of Rho GTPase activities during cell protrusion, Nature (London) **461**, 99 (2009).
[37] J. E. Ron, J. d'Alessandro, V. Cellerin, R. Voituriez, B. Ladoux, and N. S. Gov, Polarization and motility of one-dimensional multi-cellular trains, Biophys. J. **122**, 4598 (2023).
[38] T. Bertrand, J. d'Alessandro, A. Maitra, S. Jain, B. Mercier, R.-M. Mège, B. Ladoux, and R. Voituriez, Clustering and ordering in cell assemblies with generic asymmetric aligning interactions, Phys. Rev. Res. **6**, 023022 (2024).
[39] A. C. Callan-Jones and R. Voituriez, Actin flows in cell migration: From locomotion and polarity to trajectories, Curr. Opin. Cell Biol. **38**, 12 (2016).
[40] R. J. Hawkins, R. Poincloux, O. Bénichou, M. Piel, P. Chavrier, and R. Voituriez, Spontaneous contractility-mediated cortical flow generates cell migration in three-dimensional environments, Biophys. J. **101**, 1041 (2011).
[41] C. A. Wilson, M. A. Tsuchida, G. M. Allen, E. L. Barnhart, K. T. Applegate, P. T. Yam, L. Ji, K. Keren, G. Danuser, and J. A. Theriot, Myosin II contributes to cell-scale actin network treadmilling through network disassembly, Nature (London) **465**, 373 (2010).
[42] C. Jurado, J. R. Haserick, and J. Lee, Slipping or gripping? Fluorescent speckle microscopy in fish keratocytes reveals two different mechanisms for generating a retrograde flow of actin, Mol. Biol. Cell **16**, 507 (2005).
[43] M. Dembo and Y.-L. Wang, Stresses at the cell-to-substrate interface during locomotion of fibroblasts, Biophys. J. **76**, 2307 (1999).
[44] Z. Messi, A. Bornert, F. Raynaud, and A. B. Verkhovsky, Traction forces control cell-edge dynamics and mediate distance sensitivity during cell polarization, Curr. Biol. **30**, 1762 (2020).
[45] M. Lekka, K. Gnanachandran, A. Kubiak, T. Zieliński, and J. Zemła, Traction force microscopy—Measuring the forces exerted by cells, Micron **150**, 103138 (2021).
[46] N. Ibata and E. M. Terentjev, Development of nascent focal adhesions in spreading cells, Biophys. J. **119**, 2063 (2020).
[47] C. Cadart, E. Zlotek-Zlotkiewicz, L. Venkova, O. Thouvenin, V. Racine, M. L. Berre, S. Monnier, and M. Piel, Fluorescence exclusion measurement of volume in live cells, Methods Cell Biol. **139**, 103 (2017).